ACS OMEGA

http://pubs.acs.org/journal/acsodf

Article

Mutation in Transmembrane Domain 8 of Human Urate Transporter 1 Disrupts Uric Acid Recognition and Transport

Qunsheng Lan, Ze'an Zhao, Hui Liao, Fengxin Zheng, Yongjun Chen, Ting Wu, Yuanxin Tian,* and Jianxin Pang*

Cite This: *ACS Omega* 2022, 7, 34621−34631

Read Online

ACCESS | Metrics & More | Article Recommendations

ABSTRACT: Human urate transporter 1 (hURAT1) is the most pivotal therapeutic target for hyperuricemia. Due to a lack of crystal structure information, the atomic structure of URAT1 is not clearly understood. In this study, a multiple sequence alignment was performed, and K393, a positively charged residue in transmembrane domain (TMD) 8, was observed to be highly conserved in organic anion transporters (OATs). K393 was substituted with a positively, negatively, and neutrally charged amino acid via site-directed mutagenesis and then used to transfect HEK293 cells. Reverse transcription-quantitative polymerase chain reaction (RT-qPCR) and enzyme-linked immunosorbent assay (ELISA) analyses indicated that mutants of K393 showed mRNA and protein expression levels similar to those in the WT group. The nonpositively charged mutants K393A, K393D, and K393E eliminated 70−80% of ^{14}C-uric acid transport capacity, while the K393H mutant showed slight and the K393R mutant showed no reduced transport capacity compared with the WT group. Binding assays indicated that K393A, K393D, and K393E conferred lowered uric acid binding affinity. As indicated by the K_m and V_{max} values obtained from saturation kinetic experiments, K393A, K393D, and K393E showed increased K_m values, but K393R and K393H showed K_m values similar to those in the WT group. K393 also contributed to a high affinity for benzbromarone (BM) interaction. The inhibitory effects of BM were partly abolished in K393 mutants, with increased IC_{50} values compared with the WT group. BM also exhibited weaker inhibitory effects on ^{14}C-uric acid binding in K393R and K393H mutants. In an outward homology model of URAT1, K393 was located in the inner part of the transport tunnel, and further molecular docking analysis indicated that uric acid and BM showed possible hydrogen bonds with K393. Mutants K393R and K393H showed possible interactions with uric acid, and positive charges confer high affinity for uric acid as revealed by their surface electrostatic potential. In conclusion, our data provide evidence that K393 is an important residue for the recognition of uric acid or inhibitors by URAT1.

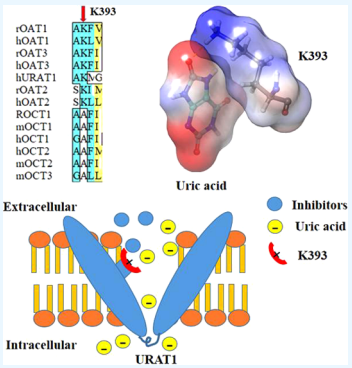

1. INTRODUCTION

Hyperuricemia and gout occur when there is an excess of uric acid (urate) in the blood (serum uric acid > 6.8 mg/dL).[1] Hyperuricemia is regarded as a novel dangerous metabolic disease after hypertension,[2] diabetes,[3] and hyperlipidemia.[4] The serum urate level is kept in balance between secretion and reabsorption by various urate transporters in the kidney and intestine (mainly in the kidney). These transporters include urate reabsorption transporter 1 (URAT1, SLC22A12), glucose transporter 9 (GLUT9, SLC2A9),[5] and organic anion transporters 4/10 (SLC22A11/13),[6] which are responsible for reabsorption of uric acid into blood. In contrast, organic anion transporters 1/3 (OAT1/3, SLC22A6/8)[7] and ATP-binding cassette subfamily G member 2 (ABCG2)[8] are responsible for secretion of uric acid into urine.

URAT1 is the most important urate transporter and mediates 90% of the reabsorption of urate in the kidney.[9] In 2015, the first URAT1 inhibitor, lesinurad,[10] was approved and put on the market for the treatment of hyperuricemia. However, considering its poor efficacy, it was only approved in combination with XOD inhibitors, such as allopurinol.[11] A lack of structural information has limited novel skeleton drug development and screening, and thus, only a few URAT1 inhibitors, such as verinurad[12] and dotinurad,[13] have been approved for clinical experiments, and they are all analogues of existing drugs. A better understanding of the three-dimensional (3D) structure and active sites of URAT1 is urgent to design selective urate-lowering drugs targeting URAT1. For example, Peng[14] and Ao[15] discovered potential URAT1 inhibitors, and the binding mode was predicted using a homology model. However, the details of the URAT1 transport mechanism have not been fully disclosed.

Received: July 19, 2022
Accepted: September 7, 2022
Published: September 15, 2022

https://doi.org/10.1021/acsomega.2c04543
ACS Omega 2022, 7, 34621−34631

URAT1 is a member of the organic anion transporter (OAT) family, which is a subfamily of the major facilitator superfamily (MFS).[16] OATs are homologous proteins with similar amino acid sequences and share similar secondary topology structures: 12 transmembrane domains (TMDs), an extracellular loop between TMDs 1 and 2, and an intracellular loop between TMDs 6 and 7.[17] All of the TMDs are organized into three layers from innermost to outermost, forming a three-dimensional structure, and the corresponding TMDs in each layer play similar structural and functional roles.[18] The MFS possesses similar secondary structure sequence information but has different substrates based on charge selectivity. Similar to OATs, organic cation transporters (OCTs) mediate the process of organic cation transport across the membranes of epithelia. OCTs share 30−40% sequence identity with OATs.[19] The remaining sequence differences may provide insight into the substrate specificities of the transporters.

As a negatively charged molecule, positively charged amino acids (arginine, lysine, histidine) may contribute to strong interactions with uric acid. For example, a previous sequence alignment performed with hOAT1 revealed that R466 in TMD11, a highly conserved residue in OATs, is selectively related to anion interactions. In addition, R466 in OAT1 has been verified to be a structural change−related residue.[20] In our previous report, the corresponding positively charged residue R477 in TMD11 of URAT1 was demonstrated to be related to substrate recognition and structural change.[21] Furthermore, R477 was also shown to be the binding site of the URAT1 inhibitors verinurad (RDEA3170) and BM.[22]

In this study, K393 in TMD8 of URAT1 was found to be another conserved alkaline amino acid, similar to R477, as observed by multiple sequence alignment of OATs and OCTs. The results indicated that the positive charge or alkalinity of K393 is essential for the interaction of URAT1 with uric acid. K393 is also a potential binding residue for URAT1 inhibitors. Our results suggest that K393 plays an important role in both uric acid and inhibitor interactions, and we hope our findings can help in further exploration of the details underlying the uric acid/URAT1 interaction and provide insight into other transporters.

2. EXPERIMENTAL PROCEDURES

2.1. Materials. RDEA3170 (verinurad) was obtained from HWRK Biotech Company (Beijing, China). Other compounds and reagents were analytical grade and purchased from Sigma (St. Louis, MO).^{14}C-labeled uric acid (55 mCi/mmol) was obtained from American Radiolabeled Chemicals Inc. (ARC, Missouri), and poly-D-lysine (PDL) was purchased from Beyotime Biotechnology (Shanghai, China). The polymerase chain reaction (PCR) mix was purchased from Vazyme Biotech Company (Nanjing, China). The N-Flag-hURAT1-pECFP plasmid and pECFP empty vector were purchased from Youze Biotech Company (Changsha, China).

2.2. Cell Culture. Human embryonic kidney 293 (HEK293) cells were cultured in DMEM supplemented with 10% fetal bovine serum (ExCell Bio, Shanghai, China), 100 units/mL penicillin, and 100 mg/mL streptomycin. Cells were kept at 37 °C in an incubator with 5% CO_2.

2.3. Sequence Alignment and Two-Dimensional (2D) Topology Prediction. The secondary sequences of OATs (hURAT1, hOAT1, hOAT2, hOAT3, rOAT1, rOAT2, and rOAT3) and OCTs (hOCT1, hOCT2, mOCT1, mOCT2, and mOCT3) were obtained from the NCBI database in the fasta format, and the sequences were uploaded to the PROMALS3D alignment web server.[23] The conservation information is shown in the figure, and relatively conserved residues were scanned. URAT1 amino acid information was uploaded to the topology prediction web servers HMMTOP[24] and TMHMM,[25] and the predicted secondary structure and topology of URAT1 were displayed using the TOPO2 web server (http://www.sacs.ucsf.edu/TOPO2/).

2.4. Site-Directed Mutagenesis of hURAT1. The N-Flag-hURAT1-pECFP plasmid was used as a PCR template, and specific mutants were generated via site-directed mutagenesis using superfidelity DNA polymerase (Vazyme, Nanjing, China). The PCR procedure was performed according to the instructions. Primers were designed using Snapgene 2.3 software and synthesized by Tsingke Biotech Company (Beijing, China). The detailed primer sequence information is displayed in Table 1. The PCR end product was digested with Dpn1 enzyme (Takara, Shanghai, China) overnight and transferred to DH5α competent cells (New Cell and Molecular Biotech, Suzhou, China). Mutants were selected on solid LB medium with kanamycin, and then, sequences were confirmed with a 3100 automatic sequencing analyzer (Applied Biosystems, Foster City, CA).

Table 1. Primers Used for Site-Directed Mutagenesis

mutation	primers
K393A forward	5′-ATCCCAGCCGCCATGGGC-3′
K393A reverse	5′-GCCCATGGCGGCTGGGAT-3′
K393D forward	5′-ATCCCAGCCGACATGGGC-3′
K393D reverse	5′-GCCCATGTCGGCTGGGAT-3′
K393E forward	5′-ATCCCAGCCGAAATGGGC-3′
K393E reverse	5′-GCCCATTTCGGCTGGGAT-3′
K393R forward	5′-ATCCCAGCCCGCATGGGC-3′
K393R reverse	5′-GCCCATGCGGGCTGGGAT-3
K393H forward	5′-ATCCCAGCCCACATGGGC-3′
K393H reverse	5′-GCCCATGTGGGCTGGGAT-3′

2.5. Mutant Extraction and Transfection. The confirmed mutant plasmids were extracted using a plasmid extraction kit (Foregene, Chengdu, China) following the manufacturer's instructions. Then, HEK293 cells were transiently transfected with the plasmids using Lipofectamine 3000 (Invitrogen, CA). In brief, cells were seeded into 24-well plates at a density of 1×10^5 cells/well. When the cells reached 70% confluence, a mixture of 0.75 μL of Lipo3000 and 500 ng of DNA (WT or mutants) was added to the plates. After 24 h, relative mRNA and protein expression levels were detected by RT-qPCR and enzyme-linked immunosorbent assay (ELISA), respectively, and ^{14}C-uric acid uptake assays or kinetic experiments were performed.

2.6. ^{14}C-Uric Acid Uptake Assay. HEK293 cells were seeded into poly-D-lysine (PDL)-coated 96-well plates at a density of 1×10^5 cells/well. HEK293 cells were transiently transfected with the URAT1 plasmid or empty vector (100 ng/well) using Lipofectamine 3000. After transfection for 24 h, the cells were incubated with uric acid uptake buffer for 30 min as we previously reported,[26] with or without the tested compounds at various concentrations. The uptake was initiated by adding ^{14}C-uric acid at a final concentration of 25 μM for 15 min. The cells were then washed three times with ice-cold DPBS to terminate the reaction. Cell lysates were obtained by adding 100 μL of 0.1 M sodium hydroxide. Intracellular

https://doi.org/10.1021/acsomega.2c04543
ACS Omega 2022, 7, 34621−34631

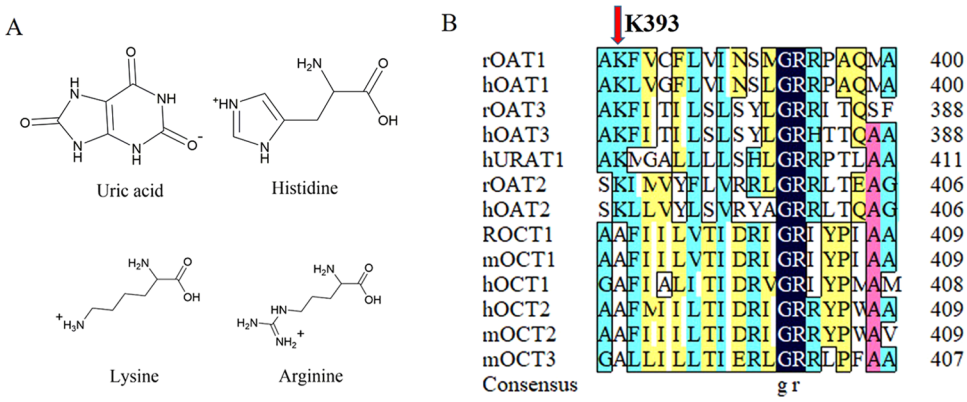

Figure 1. Positively charged K393 in URAT1 is highly conserved. (A) Structure of uric acid and positively charged amino acids. (B) Multiple sequence alignment of OATs and OCTs.

radioactivity was determined using a liquid scintillation counter (PerkinElmer, Boston, MA) after addition of 0.5 mL of scintillation fluid. Experiments were performed in triplicate. The inhibition rates of the tested compounds were calculated as follows:

$$\text{specific inhibition} = [1 - (\text{CPMt} - \text{CPM0}) / (\text{CPMmod} - \text{CPM0})] \times 100\%$$

where CPMt is the radioactivity of the tested group and CPMmod is the intracellular radioactivity of the model (untreated) group. CPM0 is the intracellular radioactivity of the cells transfected with empty vector without hURAT1.

2.7. Saturation Kinetic Experiment. HEK293 cells transfected with hURAT1 or its mutants were incubated with the uptake buffer for 15 min. Then, different concentrations of pure ^{14}C-uric acid (10−200 μM) were added to initiate the uptake for 20 min. In the kinetics studies of the WT and various hURAT1 mutant groups, the endogenous uptake was subtracted, and the results were corrected by the uptake in the mock group transfected with empty vector (about 10−15% of the WT group). The K_m and V_{max} values were determined from Michaelis−Menten plots.

2.8. Binding Assay. Membrane protein was prepared from transfected HEK293 cells expressing mutants in 100 mm cell dishes. The protein of the control group was prepared from transfected HEK293 cells expressing pECFP empty vector. In brief, cells were harvested in 1 mL of ice-cold binding buffer (25 mM HEPES, pH 7.3, 125 mM sodium gluconate). Cells were broken with a zigzag centrifuge tube, and membrane protein was extracted according to the manufacturer's instructions (Invent, Beijing, China). To initiate binding, membranes (2.5 μg total protein) were incubated with 25 μM ^{14}C-uric acid without or with an inhibitor for 30 min at room temperature. The samples were then rapidly filtered through 0.45 μM filter tubes (Millipore, Massachusetts) and washed with ice-cold DPBS. The complex sediments were dissolved with 0.1 M NaOH. After addition of 0.5 mL of scintillation fluid, the samples were subjected to a scintillation counter (PerkinElmer, Boston, MA).

2.9. ELISA Analysis of the Membrane Localization of K393 Mutants. To quantitatively detect the membrane localization of mutants and exclude endogenous URAT1, Flag-URAT1-pECFP plasmids were used in combination with ELISA-based methods. The procedures were as follows: HEK293 cells were transfected with 500 ng/well N-terminal Flag-tagged URAT1 or empty vector in 24-well plates. Twenty-four hours after transfection, the cells were washed with TBS solution and fixed with paraformaldehyde for 15 min. Then, the cells were blocked with 1% bovine serum albumin (BSA) for 1 h. After that, the cells were incubated with anti-Flag monoclonal antibody (1:2000, Solarbio, Beijing, China) for 2 h at room temperature followed by three washes with TBS solution. Next, the cells were incubated in TBS solution containing BSA (1%) and HRP-anti-rabbit IgG (1:5000) at room temperature for 1 h and then washed with TBS solution three times. Finally, 150 μL of the HRP substrate tetramethylbenzidine (Solarbio, Beijing, China) was added and incubated with the cells for 20 min at room temperature, and 150 μL of 1 M H_2SO_4 was added to stop the reaction. The absorbance was determined at 450 nM using a microplate reader.

2.10. RT-qPCR. HEK293 cells were transfected with the appropriate plasmids for 24 h, and then, total RNA was extracted from the cells using an RNA isolation kit (Foregene, Chengdu, China). Subsequently, 500 ng of total RNA was reverse transcribed to cDNA using PrimeScript RT Master Mix (TaKaRa, Japan). The mRNA levels were determined using PowerUp SYBR Green Master Mix (Thermo Fisher Scientific) on a Roche LightCycler 480II system (Roche, Switzerland). The mRNA levels of target genes were normalized to those of the β-actin gene. The relative mRNA expression levels of transporters were calculated using the $2^{-\Delta\Delta Ct}$ method.

2.11. Molecular Docking. Due to the lack of reported 3D structural information for URAT1, we used an outward homology model of URAT1, and docking experiments were performed using the Schrödinger Induced Fit Docking (IFD) protocol as we previously reported.[21] In brief, compounds were constructed with a 2D sketcher, and their 3D structures were prepared using LigPrep to generate plausible ionization and tautomerization states at pH 7. The K393 residue was considered the center of the binding site. IFD was carried out with the default parameters for the best hits using OPLS3 as the energy minimization force field. The initial docking poses within 30.0 kcal/mol of the top ranking were redocked using the Glide XP Visualizer panel. K393 was virtually mutated to alanine (A), aspartic acid (D), glutamic acid (E), arginine (R), and histidine (H), followed by structure optimization and docking. The positions with the highest ranking docking scores are reported here to demonstrate the binding details. The binding energy was analyzed using the MMGBSA module. Surfaces were generated surrounding K393

https://doi.org/10.1021/acsomega.2c04543
ACS Omega 2022, 7, 34621−34631

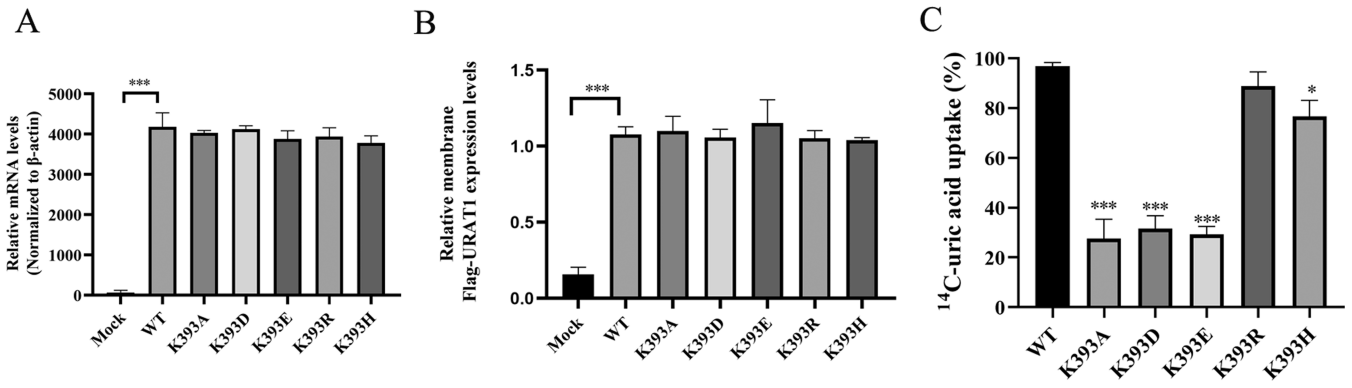

Figure 2. Effects of K393 on ^{14}C-uric acid transport. (A) Relative mRNA expression levels of K393 mutants. (B) Relative membrane Flag-URAT1 protein levels of K393 mutants. (C)^{14}C-Uric acid uptake of K393 mutants and URAT1 in HEK293 cells. $n = 3$. The data are expressed as the mean ± SD. *$P < 0.05$, ***$P < 0.001$ compared with the WT group.

and mutants interacting with uric acid. The electrostatic potential of the surface negative charge (red) and positive charge (blue) and the potential electrostatic interactions between uric acid and the K393 mutants were further displayed.

2.12. Data Analysis. Values are expressed as the mean ± SD. The kinetic parameters (apparent K_m and V_{max}) were determined by the Michaelis−Menten equation using GraphPad version 8.0. Statistical analysis of the data was carried out with an unpaired t test, where $P < 0.05$ was considered significant. For multiple groups comparisons, statistical significance analysis was performed using one-way analysis of variance (ANOVA) followed by Tukey's multiple pairwise comparisons test using GraphPad version 8.0.

3. RESULTS

3.1. K393 is Highly Conserved in OATs. Substrates of OATs generally carry negative charge(s), whereas substrates of OCTs are cations. As an organic anion, uric acid carries a negative charge and might interact with positively charged residues. To elucidate the possible functional and pivotal amino acids in URAT1, we focused on the positively charged amino acids in URAT1, including histidine, arginine, and lysine (Figure 1A). Multiple sequence alignment (MSA) of OATs and OCTs was performed, and the results indicated that there are two conserved residues, R477 in TMD11 and K393 in TMD8, that exhibited the reverse property between OATs and OCTs. The amino acids in the OCTs in the positions corresponding to R477 were negatively charged aspartic acid (D). A previous report indicated that R477 is an important residue related to uric acid transport, inhibitor binding, and structural changes in URAT1.[22,27]

In this study, K393 attracted our attention. We hypothesized that K393 may also be important in substrate discrimination between anions and cations. As shown in the multiple sequence alignment (Figure 1B), K393 was conserved, and the residues in the corresponding positions in OATs were lysine (K) but were noncharged alanine residues (A) in OCTs (red arrow). Considering the anion selectivity of URAT1, K393 might play an important role in recognition of uric acid by URAT1, which deserves further investigation.

3.2. K393 is Important in ^{14}C-Uric Acid Transport Mediated by URAT1. To gain insight into the functional role of residue K393 in uric acid transport, mutants of K393 substituted with positively, negatively, or neutrally charged amino acids, including alanine (A), aspartic acid (D), glutamic acid (E), arginine (R), and histidine (H), were generated. To investigate whether mutants of K393 could affect membrane anchoring and expression, HEK293 cells were transfected with mutants to confer expression. RT-qPCR results indicated that the mRNA expression levels were not affected after the mutation (Figure 2A). Membrane anchoring levels were evaluated by quantifying N-terminal Flag using ELISAs. The results indicated that the membrane protein localization of the K393 mutants was not affected compared with that in the WT group (Figure 2B).

Then, a ^{14}C-uric acid uptake assay was conducted in K393 mutants and wild-type URAT1. The results indicated that when K393 was mutated to alanine (A) or to the reversely charged amino acids aspartic acid (D) and glutamic acid (E), approximately 70−80% of the ^{14}C-urate transport capacity of URAT1 was lost compared with that in the WT group. The positively charged mutant K393R showed no reduction in ^{14}C-uric acid transport, and K393H showed a slightly reduced transport capacity compared with that of the WT (Figure 2C). This result indicates that K393 is important in ^{14}C-uric acid transport.

To investigate the detailed role of K393 in uric acid transport, further kinetic experiments were conducted in HEK293 cells. The results indicated that the negatively and neutrally charged mutants K393A, K393D, and K393E showed lowered affinity for uric acid, with significantly increased K_m values (165.36−201.23 μM) compared with the WT group (106.45 μM). They also showed reduced V_{max} values (424.14−497.21 μM) compared with the wild-type group (654.12 μM), suggesting that the transport velocity was blunted after the mutation. The positively charged mutants K393R and K393H showed K_m values (128.11 and 101.23 μM, respectively) similar to those of the WT group (106.45 μM). In conclusion, the positive charge of K393 confers high affinity for uric acid binding (Table 2).

The mutant K393R showed K_m and V_{max} values similar to those of the WT group, which indicated that the positive charge is important. However, although histidine carries a positive charge, it was noted that the mutant K393H also showed a slightly increased but not significant K_m value ($P > 0.05$) and a reduced V_{max} value ($P < 0.01$) compared with the WT group. As shown in Figure 1A, histidine has a positive imidazole group, while lysine has a long side chain similar to arginine. The side chain of lysine is extremely different from

https://doi.org/10.1021/acsomega.2c04543
ACS Omega 2022, 7, 34621−34631

Table 2. Kinetic Parameters of ^{14}C-Uric Acid uptake by URAT1 and K393 Mutants[a]

Mutants	K_m (μM)	V_{max} (pmol/min·mg)
WT	106.45 ± 16.45	654.12 ± 102.14
K393A	172.12 ± 27.12**	464.25 ± 89.23*
K393D	165.36 ± 23.41**	497.21 ± 85.5*
K393E	201.23 ± 23.65**	424.14 ± 61.22**
K393H	128.11 ± 19.12 (ns)	447.12 ± 43.21**
K393R	101.23 ± 26.11 (ns)	557.21 ± 89.21(ns)

[a]n = 3. The data are expressed as the mean ± SD; ns, not significant. *P < 0.05, **P < 0.01 compared with the WT group.

that of histidine. A possible reason is that the lower base strength of the imidazole side chain of K393H is weaker so that it cannot form as strong of a bond with organic anions as K393R; therefore, its affinity for anionic substrates is lower, but still substantially higher than the nonbasic mutants.

3.3. K393 is Important for Uric Acid Binding/Transport. URAT1 is a high-affinity urate transporter, and K393 plays an important role in uric acid binding and transport. To further verify the direct effect of K393 on uric acid binding and transport, a competitive inhibition test of unlabeled uric acid was performed as previously reported[22] with a little modification. HEK293 cells overexpressing URAT1 or K393 mutants were incubated with unlabeled uric acid for 30 min (the unlabeled uric acid untreated groups performed as control). After that, extracellular uric acid solution was removed and cells were then washed with DPBS to clean the uncombined uric acid. And then,^{14}C-uric acid uptake was initiated for 15 min. The results indicated that unlabeled uric acid inhibited the transport of ^{14}C-uric acid in the WT group with an IC_{50} value of 115.30 ± 6.36 μM. Unlabeled uric acid inhibited the ^{14}C-uric acid uptake of K393R and K393H with IC_{50} values of 112.54 ± 10.12 and 121.20 ± 5.98 μM, respectively, which are similar to that in the WT group (Figure 3A). This indicated that replacement of K393 with positively charged residues has little effect on uric acid binding and transport of URAT1. Notably, the mutants K393A, K393D, and K393E lost most of their uric acid transport capacity compared with the WT group. These mutants retained poor uric acid uptake capacity, and thus, they were not able to fit the convincing IC_{50} values of unlabeled uric acid.

To further explore the importance of the positive charge of K393, the membrane proteins of cells expressing URAT1 and K393 mutants were extracted, and 2.5 μg of protein solution was incubated with 25 μM ^{14}C-uric acid for 30 min. As shown in Figure 3B, the K393H and K393R mutants showed a binding capacity similar to that in the WT group, while the K393A, K393D, and K393E mutants showed significant loss in uric acid binding. In conclusion, K393 has a direct interaction with uric acid, and its positive charge confers high affinity for uric acid.

3.4. K393 Confers High Affinity for BM Binding. Next, we investigated whether K393 contributes to the high affinity for inhibitors. Several commercially available URAT1 inhibitors, including BM,[28] lesinurad,[29] verinurad (RDEA3170), and probenecid,[30] were used. A ^{14}C-uric acid uptake assay was conducted in HEK293 cells, and the URAT1 inhibition effects of these compounds were tested in WT, K393R, and K393H mutants. As shown in Table 3, verinurad, lesinurad, BM, and probenecid inhibited URAT1 with IC_{50} values of 0.29, 6.94, 0.22, and 20.21 μM, respectively. Among them, lesinurad, verinurad, and probenecid inhibited K393 mutants with IC_{50} values similar to those of the WT group. BM showed significantly increased IC_{50} values in the K393 mutants. This finding suggests that the inhibitory effects of BM on URAT1 were partly eliminated after the mutation.

Consistent with this observation, a competitive binding test of inhibitors and ^{14}C-uric acid was performed. According to the IC_{50} values of each URAT1 inhibitor, the protein was incubated with 1 μM BM, 1 μM verinurad, 10 μM lesinurad, and 20 μM probenecid for 30 min, and then, 25 μM ^{14}C-uric acid was added. Uncombined ^{14}C-uric acid was removed, and ^{14}C-uric acid binding was detected. As shown in Figure 4, the incubation with verinurad, lesinurad, and probenecid in the K393H and K393R groups led to similar ^{14}C-uric acid binding compared with the WT group. However, BM poorly interfered with ^{14}C-uric acid binding in K393H and K393R compared with the WT group, indicating that K393 is a pivotal binding site of BM. Additionally, there may also be other inhibitors that can interact with K393 deserving further investigation.

3.5. Molecular Docking Interaction with Inhibitors and Uric Acid. In the following experiments, an outward URAT1 homology model was used as a tool to further understand the molecular interactions between K393 and uric acid and inhibitors. As shown in Figure 5A, in the outward

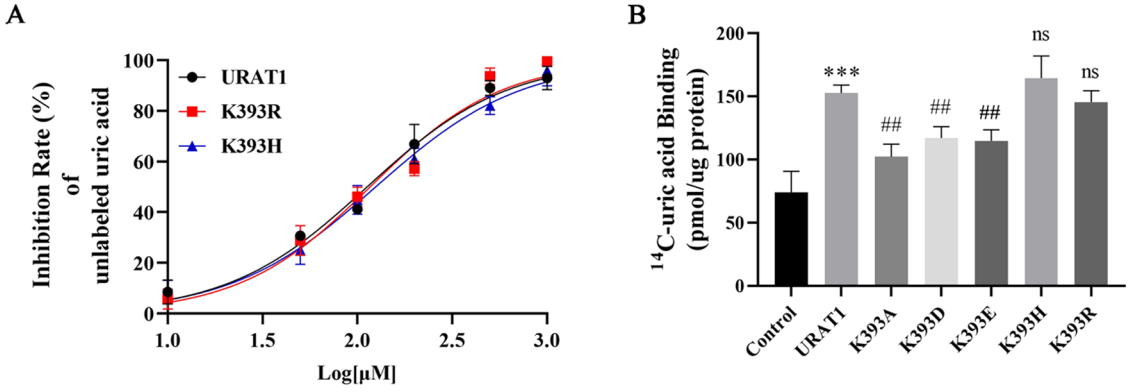

Figure 3. Binding and transport of K393 with uric acid. (A) Inhibitory effects of unlabeled uric acid on ^{14}C-uric acid transport in the K393R and K393H mutants. (B) ^{14}C-Uric acid binding capacity assays of K393 mutants in HEK293 cells. ns, not significant. ***P < 0.001 compared with the control group. ##P < 0.01 compared with the URAT1 group.

https://doi.org/10.1021/acsomega.2c04543
ACS Omega 2022, 7, 34621−34631

Table 3. IC_{50} Values of URAT1 Inhibitors in Wild-Type hURAT1 and K393 Mutants[a]

	IC_{50} (μM, mean ± SD)					
compound	WT	K393R	K393H	K393A	K393D	K393E
verinurad	0.29 ± 0.12	0.31 ± 0.29	0.49 ± 0.24	0.42 ± 0.26	0.44 ± 0.21	0.36 ± 0.22
lesinurad	6.94 ± 2.41	6.04 ± 1.62	8.79 ± 1.26	9.45 ± 4.51	8.57 ± 2.65	7.89 ± 3.66
BM	0.22 ± 0.14	1.65 ± 0.54***	1.56 ± 0.34***	1.12 ± 0.44*	3.02 ± 0.98***	1.14 ± 0.92*
probenecid	20.21 ± 2.22	18.85 ± 2.25	22.36 ± 5.22	26.98 ± 9.25	24.59 ± 5.98	22.45 ± 6.66

[a]n = 8. The data are expressed as the mean ± SD. *P < 0.1, ***P < 0.001 compared with the WT group.

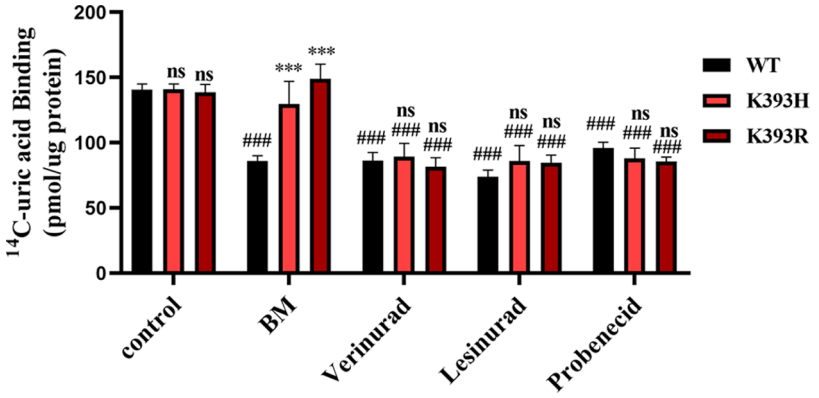

Figure 4. Competitive binding test of inhibitors and ^{14}C-uric acid in membrane proteins from cells expressing URAT1 and K393 mutants. n = 3. The data are expressed as the mean ± SD. ***P < 0.001 compared with the WT group. ns, not significant, P > 0.05 compared with the WT group. ###P < 0.001 compared with the control group (without inhibitor).

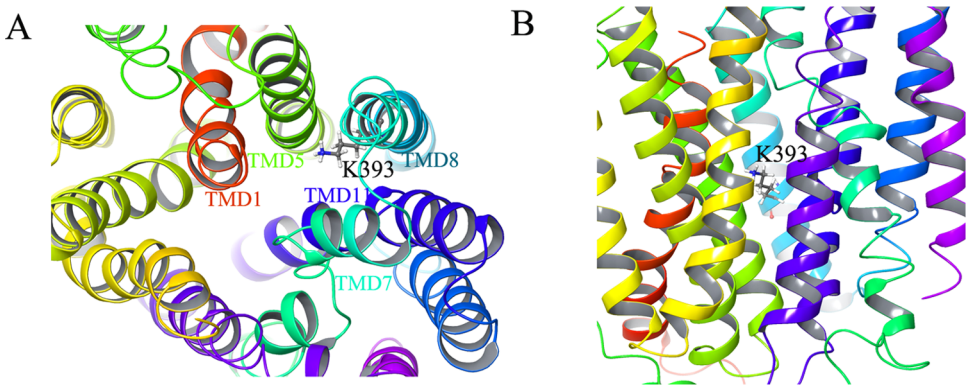

Figure 5. Vertical and horizontal perspective views of K393 in the uric acid transport tunnel in the outward URAT1 homology model. (A) Vertical view. (B) Horizontal view.

model, K393 was located in a transport tunnel composed of TMDs 1, 5, 8, and 11. The positive side-chain group of K393 faced into the tunnel. From a horizontal perspective, K393 is located in the middle portion of the tunnel (Figure 5B).

Next, molecular docking was performed, and uric acid and inhibitors were docked into a binding pocket surrounding residue K393. The docking scores and ΔG binding energy are displayed in Table 4. The docking results indicated that uric acid showed possible hydrogen bonds with K393 in TMD8 and with F449 and T450 in TMD10. Consistent with our experimental results, BM also showed possible hydrogen bonds with K393. Uric acid and BM showed possible competitive interactions with K393. In addition, BM showed a possible $\pi-\pi$ interaction with F449, a reported binding site of BM confirmed by site-directed mutation[27] (Figure 6A,B). However, other inhibitors, such as probenecid, verinurad, and lesinurad, showed no possible interaction with K393. These inhibitors showed possible interactions with multiple other

Table 4. Molecular Docking Analysis of URAT1 with Uric Acid and Inhibitors[a]

compound	binding sites	docking score	ΔG binding energy (kcal·mol^{-1})
uric acid	K393, F449, T450	−10.36	−56.85
BM	K393, F449, F358	−12.62	−78.87
probenecid	F241,W357, R477	−9.04	−70.65
verinurad	R477, F241, F358	−12.85	−78.98
lesinurad	W357, N39, R487	−9.81	−71.25

[a]Docking scores and binding energy were predicted by Schrödinger IFD. The positions with the highest ranking docking scores are reported here to demonstrate the binding details.

https://doi.org/10.1021/acsomega.2c04543
ACS Omega 2022, 7, 34621−34631

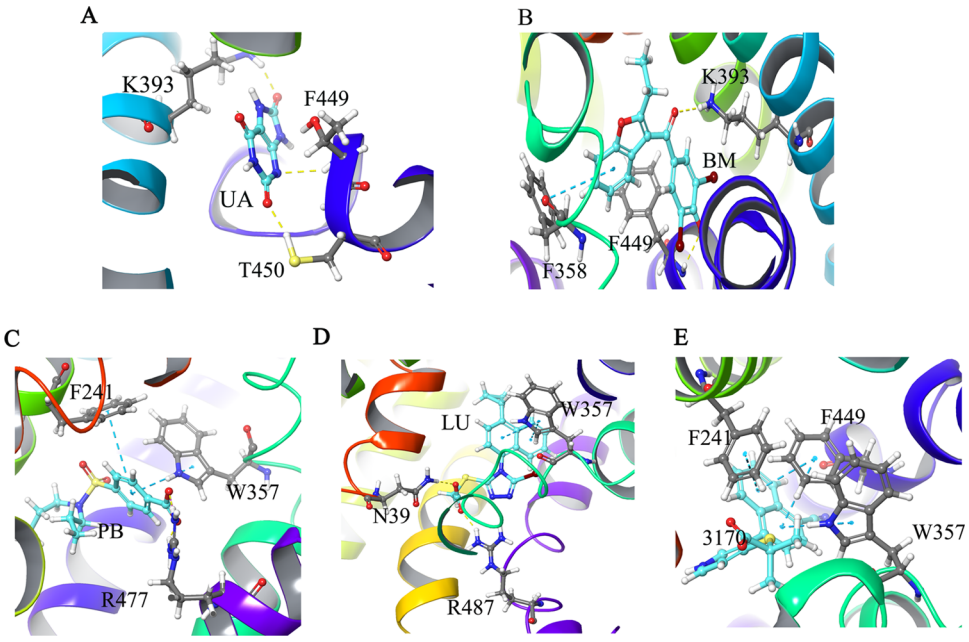

Figure 6. Binding modes of uric acid and inhibitors with URAT1 predicted by molecular docking. Schematic representation of possible interactions of hURAT1 with uric acid (A) and the inhibitors BM (B), probenecid (C), lesinurad (D), and verinurad (E).

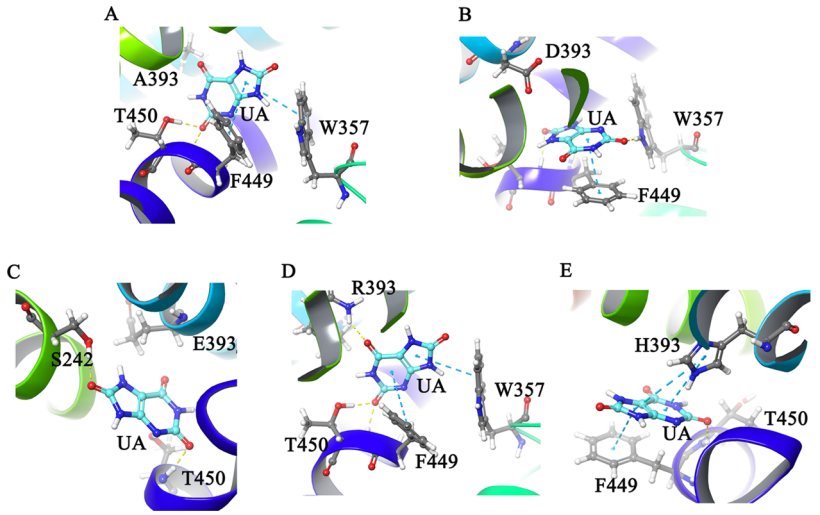

Figure 7. 3D binding modes of K393 mutants with uric acid. K393 was mutated to alanine (A), aspartic acid (B), glutamic acid (C), arginine (D), or histidine (E), followed by structure optimization and docking. The positions with the highest ranking docking scores are reported here to demonstrate the binding details.

residues, such as N39 in TMD1, F241 in TMD5, W357 and F358 in TMD7, and R477 and R487 in TMD11(Figure 6C–E). The docking scores and binding energy predicted by MMGBSA were consistent with the inhibition activities of the inhibitors in vitro. In brief, verinurad and BM showed better inhibition activities, lesinurad showed modest activities, and probenecid showed weaker inhibition activities.

To further verify the role of K393 in the uric acid interaction, we then virtually mutated K393 to various amino acids. Consistent with the in vitro results, we observed that the A393, D393, and E393 mutants showed no possible interaction with uric acid (Figure 7A–C). The docking scores and binding energies revealed that these mutants have poor binding capacities compared with K393 (Table 5). R393 and H393 still showed possible hydrogen bonds and $\pi-\pi$ interaction with uric acid, respectively, (Figure 7D,E). R393 exhibited binding activities similar to those of K393. The docking score and binding energy results indicated that H393 has weaker binding

Table 5. Molecular Docking Analysis of K393 Mutants with Uric Acid[a]

mutants	binding sites	docking scores	ΔG binding energy (kcal·mol^{-1})
WT	K393, F449, T450	−10.36	−56.85
K393A	F449, T450, W357	−8.22	−42.14
K393D	F449, W357	−8.03	−44.69
K393E	T450, S242	−5.62	−49.98
K393R	R393, W357, F449,T450	−11.24	−60.24
K393H	H393,T450, F449	−9.33	−49.98

[a]Binding sites, docking scores, and binding energies as predicted by molecular docking are summarized.

https://doi.org/10.1021/acsomega.2c04543
ACS Omega 2022, 7, 34621−34631

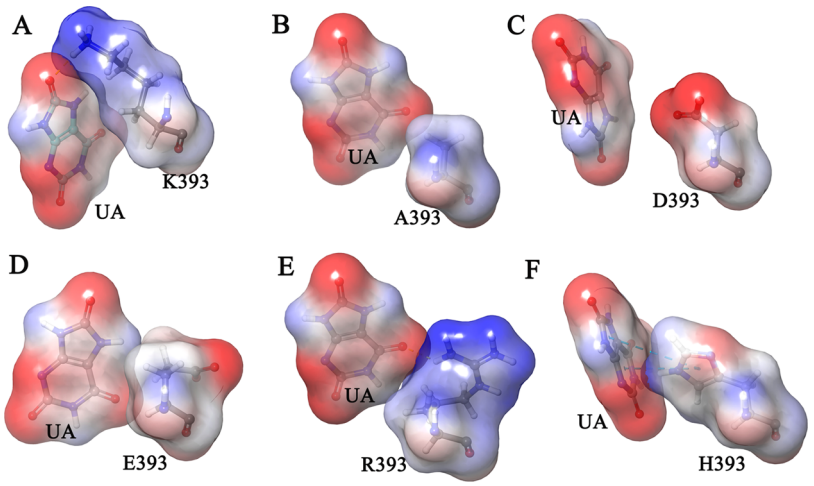

Figure 8. Surface electrostatic potential of K393 and mutants with uric acid. The surface negative charge (red) and positive charge (blue) electrostatic interaction of uric acid and WT (A), A393 (B), D393 (C), E393 (D), R393 (E), and H393 (F) mutants were performed by Schrödinger IFD.

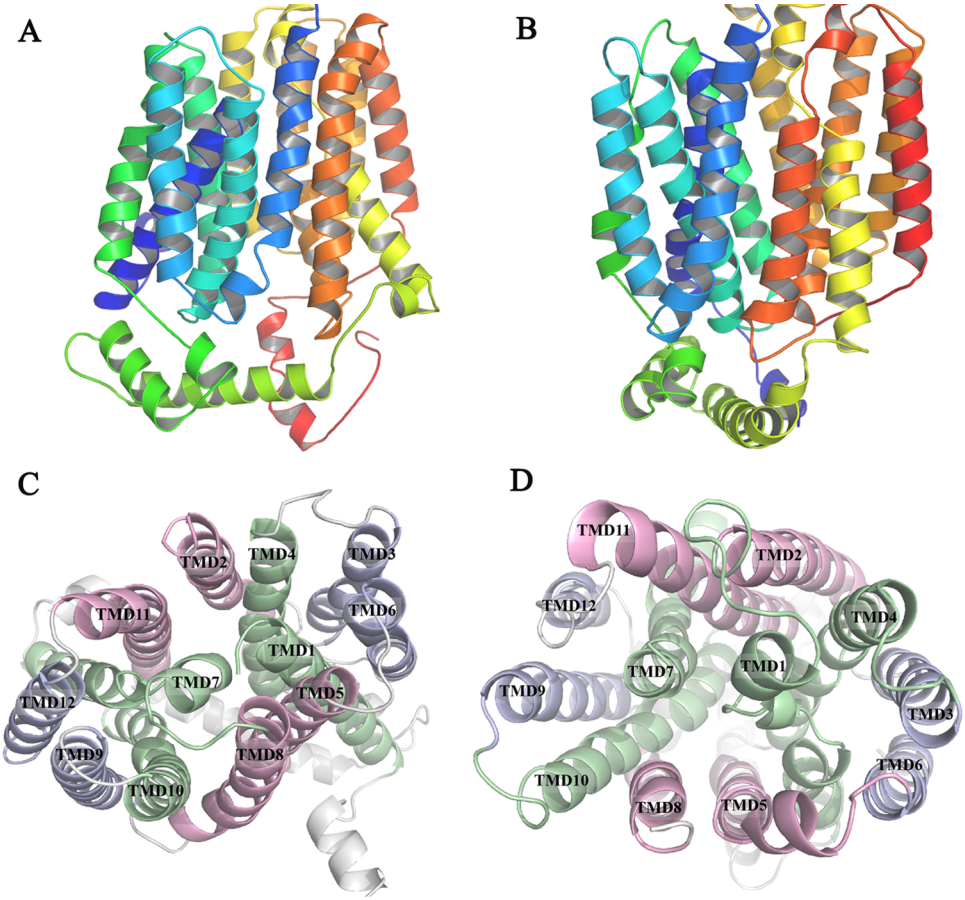

Figure 9. Schematic diagram of URAT1 inward and outward conformation exchange. (A) Horizontal view of URAT1 inward-open conformation. (B) Horizontal view of URAT1 outward-open conformation. (C) Vertical view of URAT1 inward-open conformation. (D) Vertical view of URAT1 outward-open conformation. The 3D structures were generated by homology modeling.

activity, although H393 has a possible $\pi-\pi$ stacking interaction with uric acid. One possible mechanism is that the base strength of the imidazole side chain of K393H is lower, and thus, it cannot form as strong a bond with organic anions as WT and R393.

Additionally, to investigate the role of the positive charge of K393 in the uric acid interaction, the surface electrostatic potential of K393 and mutants with uric acid was analyzed. As shown in Figure 8, the negative charge of uric acid (red) showed possible electrostatic interactions with the positive charges of K393, R393, and H393 (blue) instead of A393, D393, and E393. These results indicate that the positive charge of K393 may confer high affinity for uric acid binding.

https://doi.org/10.1021/acsomega.2c04543
ACS Omega 2022, 7, 34621−34631

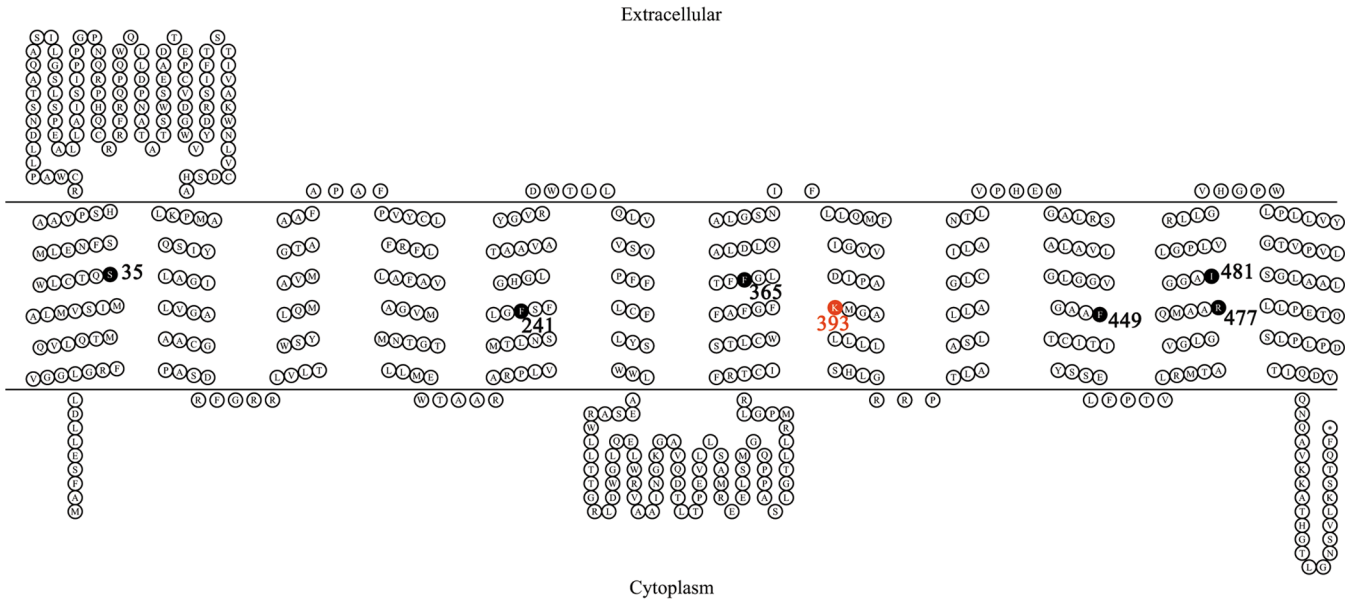

Figure 10. Summary of experimental mutations explored in URAT1. Transmembrane domains are depicted to show residue location. K393 and other reported residues conferring high affinity for uric acid and inhibitors are highlighted.

4. DISCUSSION

Hyperuricemia is mostly caused by insufficient renal urate excretion. The human urate anion transporter (hURAT1) from the SLC22 family is a unique transporter targeted by many uricosuric agents.[31] Due to the lack of a credible atomic structure, specific URAT1 inhibitors are very deficient. A better understanding of the 3D structure and the active sites is essential for designing selective urate-lowering drugs targeting hURAT1. URAT1 is a transmembrane protein, and its hydrophobic property makes it difficult to obtain a crystal structure. To date, none of the structures of urate transporters have been resolved and their substrate specificity and conformational changes have not been fully revealed.

Although there is a lack of structural information, multiple techniques, such as homology modeling, molecular docking, and multiple sequence alignment, can provide structural information that was not previously available.[32] Based on these methods, substrate recognition and structural change–related residues and domains have been partly revealed, such as in the transporters OAT1,[33] GLUT1,[34] rOCT1,[35] and rOCT2.[36] We previously developed an outward homology model of URAT1[21] and provided some insights into the uric acid transport mechanism of URAT1. We integrated multiple approaches (such as homology modeling and I-TASSER) to generate a reliable outward-open model of hURAT1. According to multiple sequence alignment of the SLC22 subfamily, structural alignment of transporters with similar function, and the probable transport mechanism, the critical active sites were disclosed. Based on the active sites, the binding modes of uric and hURAT1 inhibitors with the target were investigated via molecular docking to further understand the molecular mechanism of hURAT1 inhibitors.

Among these residues, the conserved positively charged residue R477 in TMD11 was demonstrated to be pivotal for uric acid transport. In addition, R477 was shown to be related to URAT1 binding with the inhibitors benzbormarone and verinurad by Tan PK.[27] In addition, this is not the only time that positively or negatively charged residues in the OAT/OCT family were revealed to be related to anion/cation recognition, such as R454 in rOAT3,[37] R466 in OAT1,[20] K370 in rOAT3,[37] and D475 in OCT1.[35] All of these observations suggest that we should explore more conserved positively charged residues.

URAT1 transports uric acid via inward and outward (Figure 9A,B) conformational exchange mechanisms. In this process, several TMDs undergo flexible movement and URAT1 exposes multiple binding sites to transport uric acid. It is recognized that the TMDs of the MFS family are organized into three layers, and the TMDs of each play similar structural and functional roles. The innermost TMDs 1, 4, 7, and 10 (Figure 9C,D, green colored) are located in the center of the transporter, whereas TMDs 2, 5, 8, and 11 (pink colored) are positioned outside of the innermost TMDs. All of these TMDs form a specific binding pocket for uric acid and inhibitors. The outermost TMDs 3, 6, 9, and 12 (gray colored) are involved in supporting transporter integrity. URAT1 inhibitors inhibit uric acid transport by competing with uric acid for the same binding sites. The secondary topology structure is displayed in Figure 10, and multiple residues, namely, S35 in TMD1, F241 in TMD5, F365 in TMD7, R477 in TMD11, and F449 in TMD10, were revealed to confer high affinity for inhibitors.[22,27] K393 is the first residue in TMD8 and the second positively charged residue we observed to confer high affinity for uric acid and inhibitor binding. K393 is located in the outer part of the innermost TMDs, and docking analysis indicated that the side-chain group of K393 (with a positive charge) showed a possible interaction with uric acid, and positive charges confer high affinity for uric acid as revealed by their surface electrostatic potential. We observed that when lysine was substituted with positively charged residues, the uric acid affinities were not significantly affected.

The OAT/OCT family shares a common secondary structure, and one isoform might provide insight into the binding domain of other family members. Our study supports the following major conclusions: First, K393 contributes to the uric acid recognition specificity of URAT1. Second, the positive charge and alkalinity contribute to uric acid binding. Finally, K393 is important for benzbormarone binding, and

https://doi.org/10.1021/acsomega.2c04543
ACS Omega 2022, 7, 34621−34631

K393 may confer high affinity for other URAT1 inhibitors that we have not investigated. We believe that our findings can help researchers better understand URAT1 and provide a reference for other OAT/OCT transporter studies.

AUTHOR INFORMATION

Corresponding Authors

Jianxin Pang − *Guangdong Provincial Key Laboratory of Drug Screening, School of Pharmaceutical Sciences, Southern Medical University, Guangzhou, Guangdong 510515, China;* orcid.org/0000-0002-0053-2723; Phone: +86(20)61648671; Email: pjx@smu.edu.cn

Yuanxin Tian − *Guangdong Provincial Key Laboratory of Drug Screening, School of Pharmaceutical Sciences, Southern Medical University, Guangzhou, Guangdong 510515, China;* orcid.org/0000-0003-3847-559X; Email: tyx523@163.com

Authors

Qunsheng Lan − *Department of Pharmacy, Shenzhen Longhua District Central Hospital, Shenzhen, Guangdong 518110, China*

Ze'an Zhao − *Guangdong Provincial Key Laboratory of Drug Screening, School of Pharmaceutical Sciences, Southern Medical University, Guangzhou, Guangdong 510515, China*

Hui Liao − *Guangdong Provincial Key Laboratory of Drug Screening, School of Pharmaceutical Sciences, Southern Medical University, Guangzhou, Guangdong 510515, China*

Fengxin Zheng − *Guangdong Provincial Key Laboratory of Drug Screening, School of Pharmaceutical Sciences, Southern Medical University, Guangzhou, Guangdong 510515, China*

Yongjun Chen − *Guangdong Provincial Key Laboratory of Drug Screening, School of Pharmaceutical Sciences, Southern Medical University, Guangzhou, Guangdong 510515, China*

Ting Wu − *Guangdong Provincial Key Laboratory of Drug Screening, School of Pharmaceutical Sciences, Southern Medical University, Guangzhou, Guangdong 510515, China*

Complete contact information is available at: https://pubs.acs.org/10.1021/acsomega.2c04543

Author Contributions

J.P. and Y.T.: participated in research design. Q.L., Z.Z., H.L., and T.W.: conducted experiments. H.L., Y.C., and F.Z.: performed data analysis. Q.L.: wrote or contributed to the writing of the manuscript.

Notes

The authors declare no competing financial interest.

ACKNOWLEDGMENTS

The authors thank professor Banghao Zhu and Guangyun Lin from Sun Yat-sen University for their help in ^{14}C-uric acid uptake assays. This research was funded by the Natural Science Foundation of China, grant number 81974507.

REFERENCES

(1) Dalbeth, N.; Gosling, A. L.; Gaffo, A.; Abhishek, A. Gout. *Lancet* **2021**, *397*, 1843−1855.

(2) Johnson, R. J.; Bakris, G. L.; Borghi, C.; Chonchol, M. B.; Feldman, D.; Lanaspa, M. A.; Merriman, T. R.; Moe, O. W.; Mount, D. B.; Sanchez Lozada, L. G.; Stahl, E.; Weiner, D. E.; Chertow, G. M. Hyperuricemia, Acute and Chronic Kidney Disease, Hypertension, and Cardiovascular Disease: Report of a Scientific Workshop Organized by the National Kidney Foundation. *Am. J. Kidney Dis.* **2018**, *71*, 851−865.

(3) Bartáková, V.; Kuricova, K.; Pacal, L.; Nova, Z.; Dvorakova, V.; Svrckova, M.; Maluskova, D.; Svobodova, I.; Rehorova, J.; Svojanovsky, J.; Olsovsky, J.; Belobradkova, J.; Kankova, K. Hyperuricemia contributes to the faster progression of diabetic kidney disease in type 2 diabetes mellitus. *J. Diabetes Its Complications* **2016**, *30*, 1300−1307.

(4) So, A.; Thorens, B. Uric acid transport and disease. *J. Clin. Invest.* **2010**, *120*, 1791−1799.

(5) Vitart, V.; Rudan, I.; Hayward, C.; Gray, N. K.; Floyd, J.; Palmer, C. N.; Knott, S. A.; Kolcic, I.; Polasek, O.; Graessler, J.; Wilson, J. F.; Marinaki, A.; Riches, P. L.; Shu, X.; Janicijevic, B.; Smolej-Narancic, N.; Gorgoni, B.; Morgan, J.; Campbell, S.; Biloglav, Z.; Barac-Lauc, L.; Pericic, M.; Klaric, I. M.; Zgaga, L.; Skaric-Juric, T.; Wild, S. H.; Richardson, W. A.; Hohenstein, P.; Kimber, C. H.; Tenesa, A.; Donnelly, L. A.; Fairbanks, L. D.; Aringer, M.; McKeigue, P. M.; Ralston, S. H.; Morris, A. D.; Rudan, P.; Hastie, N. D.; Campbell, H.; Wright, A. F. SLC2A9 is a newly identified urate transporter influencing serum urate concentration, urate excretion and gout. *Nat. Genet.* **2008**, *40*, 437−442.

(6) Sakiyama, M.; Matsuo, H.; Shimizu, S.; Nakashima, H.; Nakayama, A.; Chiba, T.; Naito, M.; Takada, T.; Suzuki, H.; Hamajima, N.; Ichida, K.; Shimizu, T.; Shinomiya, N. A common variant of organic anion transporter 4 (OAT4/SLC22A11) gene is associated with renal underexcretion type gout. *Drug Metab. Pharmacokinet.* **2014**, *29*, 208−210.

(7) Otani, N.; Ouchi, M.; Hayashi, K.; Jutabha, P.; Anzai, N. Roles of organic anion transporters (OATs) in renal proximal tubules and their localization. *Anat. Sci. Int.* **2017**, *92*, 200−206.

(8) Cleophas, M. C.; Joosten, L. A.; Stamp, L. K.; Dalbeth, N.; Woodward, O. M.; Merriman, T. R. ABCG2 polymorphisms in gout: insights into disease susceptibility and treatment approaches. *Pharmgenomics Pers. Med.* **2017**, *10*, 129−142.

(9) Enomoto, A.; Endou, H. Roles of organic anion transporters (OATs) and a urate transporter (URAT1) in the pathophysiology of human disease. *Clin. Exp. Nephrol.* **2005**, *9*, 195−205.

(10) Haber, S. L.; Fente, G.; Fenton, S. N.; Walker, E. P.; Weaver, B. M.; Cano, A. J.; Vu, K. Lesinurad: A Novel Agent for Management of Chronic Gout. *Ann. Pharmacother.* **2018**, *52*, 690−696.

(11) Huneycutt, E.; Board, C.; Clements, J. N. Lesinurad, a Selective URAT-1 Inhibitor With a Novel Mechanism in Combination With a Xanthine Oxidase Inhibitor, for Hyperuricemia Associated With Gout. *J. Pharm. Pract.* **2017**, 670−677.

(12) Shiramoto, M.; Liu, S.; Shen, Z.; Yan, X.; Yamamoto, A.; Gillen, M.; Ito, Y.; Hall, J. Verinurad combined with febuxostat in Japanese adults with gout or asymptomatic hyperuricaemia: a phase 2a, open-label study. *Rheumatology* **2018**, *57*, 1602−1610.

(13) Iqbal, A.; Iqbal, K.; Farid, E.; Ishaque, A.; Hasanain, M.; Bin Arif, T.; Arshad Ali, S.; Rathore, S. S.; Malik, M. Efficacy and Safety of Dotinurad in Hyperuricemic Patients With or Without Gout: A Systematic Review and Meta-Analysis of Randomized Controlled Trials. *Cureus* **2021**, *13*, No. e14428.

(14) Peng, J.; Hu, Q.; Gu, C.; Liu, B.; Jin, F.; Yuan, J.; Feng, J.; Zhang, L.; Lan, J.; Dong, Q.; Cao, G. Discovery of potent and orally bioavailable inhibitors of Human Uric Acid Transporter 1 (hURAT1) and binding mode prediction using homology model. *Bioorg. Med. Chem. Lett.* **2016**, *26*, 277−282.

(15) Ao, G. Z.; Zhou, M. Z.; Li, Y. Y.; Li, S. N.; Wang, H. N.; Wan, Q. W.; Li, H. Q.; Hu, Q. H. Discovery of novel curcumin derivatives targeting xanthine oxidase and urate transporter 1 as anti-hyperuricemic agents. *Bioorg. Med. Chem.* **2017**, *25*, 166−174.

(16) Yan, N. Structural Biology of the Major Facilitator Superfamily Transporters. *Annu. Rev. Biophys.* **2015**, *44*, 257−283.

(17) Nigam, S. K.; Bush, K. T.; Martovetsky, G.; Ahn, S. Y.; Liu, H. C.; Richard, E.; Bhatnagar, V.; Wu, W. The organic anion transporter (OAT) family: a systems biology perspective. *Physiol. Rev.* **2015**, *95*, 83−123.

https://doi.org/10.1021/acsomega.2c04543
ACS Omega 2022, 7, 34621−34631

(18) Quistgaard, E. M.; Low, C.; Guettou, F.; Nordlund, P. Understanding transport by the major facilitator superfamily (MFS): structures pave the way. *Nat. Rev. Mol. Cell Biol.* **2016**, *17*, 123−132.
(19) Nigam, S. K. The SLC22 Transporter Family: A Paradigm for the Impact of Drug Transporters on Metabolic Pathways, Signaling, and Disease. *Annu. Rev. Pharmacol. Toxicol.* **2018**, *58*, 663−687.
(20) Rizwan, A. N.; Krick, W.; Burckhardt, G. The chloride dependence of the human organic anion transporter 1 (hOAT1) is blunted by mutation of a single amino acid. *J. Biol. Chem.* **2007**, *282*, 13402−13409.
(21) Zhao, Z.; Jiang, Y.; Li, L.; Chen, Y.; Li, Y.; Lan, Q.; Wu, T.; Lin, C.; Cao, Y.; Nandakumar, K. S.; Zhou, P.; Tian, Y.; Pang, J. Structural Insights into the Atomistic Mechanisms of Uric Acid Recognition and Translocation of Human Urate Anion Transporter 1. *ACS Omega* **2020**, *5*, 33421−33432.
(22) Tan, P. K.; Liu, S.; Gunic, E.; Miner, J. N. Discovery and characterization of verinurad, a potent and specific inhibitor of URAT1 for the treatment of hyperuricemia and gout. *Sci. Rep.* **2017**, *7*, No. 665.
(23) Pei, J.; Kim, B. H.; Grishin, N. V. PROMALS3D: a tool for multiple protein sequence and structure alignments. *Nucleic Acids Res.* **2008**, *36*, 2295−2300.
(24) Tusnady, G. E.; Simon, I. The HMMTOP transmembrane topology prediction server. *Bioinformatics* **2001**, *17*, 849−850.
(25) Krogh, A.; Larsson, B.; von Heijne, G.; Sonnhammer, E. L. Predicting transmembrane protein topology with a hidden Markov model: application to complete genomes. *J. Mol. Biol.* **2001**, *305*, 567−580.
(26) Zhao, Z. A.; Jiang, Y.; Chen, Y. Y.; Wu, T.; Lan, Q. S.; Li, Y. M.; Li, L.; Yang, Y.; Lin, C. T.; Cao, Y.; Zhou, P. Z.; Guo, J. Y.; Tian, Y. X.; Pang, J. X. CDER167, a dual inhibitor of URAT1 and GLUT9, is a novel and potent uricosuric candidate for the treatment of hyperuricemia. *Acta Pharmacol. Sin.* **2022**, *43*, 121−132.
(27) Tan, P. K.; Ostertag, T. M.; Miner, J. N. Mechanism of high affinity inhibition of the human urate transporter URAT1. *Sci. Rep.* **2016**, *6*, No. 34995.
(28) Azevedo, V. F.; Kos, I. A.; Vargas-Santos, A. B.; da Rocha Castelar Pinheiro, G.; Dos Santos Paiva, E. Benzbromarone in the treatment of gout. *Adv. Rheumatol.* **2019**, *59*, 37.
(29) Miner, J. N.; Tan, P. K.; Hyndman, D.; Liu, S.; Iverson, C.; Nanavati, P.; Hagerty, D. T.; Manhard, K.; Shen, Z.; Girardet, J. L.; Yeh, L. T.; Terkeltaub, R.; Quart, B. Lesinurad, a novel, oral compound for gout, acts to decrease serum uric acid through inhibition of urate transporters in the kidney. *Arthritis Res. Ther.* **2016**, *18*, No. 214.
(30) Gafter, U.; Zuta, A.; Frydman, M.; Lewinski, U. H.; Levi, J. Hypouricemia due to familial isolated renal tubular uricosuria. Evaluation with the combined pyrazinamide-probenecid test. *Miner. Electrolyte Metab.* **1989**, *15*, 309−314.
(31) Dong, Y.; Zhao, T.; Ai, W.; Zalloum, W. A.; Kang, D.; Wu, T.; Liu, X.; Zhan, P. Novel urate transporter 1 (URAT1) inhibitors: a review of recent patent literature (2016-2019). *Expert Opin. Ther. Pat.* **2019**, *29*, 871−879.
(32) Garibsingh, R. A.; Otte, N. J.; Ndaru, E.; Colas, C.; Grewer, C.; Holst, J.; Schlessinger, A. Homology Modeling Informs Ligand Discovery for the Glutamine Transporter ASCT2. *Front. Chem.* **2018**, *6*, No. 279.
(33) Perry, J. L.; Dembla-Rajpal, N.; Hall, L. A.; Pritchard, J. B. A three-dimensional model of human organic anion transporter 1: aromatic amino acids required for substrate transport. *J. Biol. Chem.* **2006**, *281*, 38071−38079.
(34) Salas-Burgos, A.; Iserovich, P.; Zuniga, F.; Vera, J. C.; Fischbarg, J. Predicting the three-dimensional structure of the human facilitative glucose transporter glut1 by a novel evolutionary homology strategy: insights on the molecular mechanism of substrate migration, and binding sites for glucose and inhibitory molecules. *Biophys. J.* **2004**, *87*, 2990−2999.
(35) Popp, C.; Gorboulev, V.; Muller, T. D.; Gorbunov, D.; Shatskaya, N.; Koepsell, H. Amino acids critical for substrate affinity of rat organic cation transporter 1 line the substrate binding region in a model derived from the tertiary structure of lactose permease. *Mol. Pharmacol.* **2005**, *67*, 1600−1611.
(36) Zhang, X.; Shirahatti, N. V.; Mahadevan, D.; Wright, S. H. A conserved glutamate residue in transmembrane helix 10 influences substrate specificity of rabbit OCT2 (SLC22A2). *J. Biol. Chem.* **2005**, *280*, 34813−34822.
(37) Feng, B.; Dresser, M. J.; Shu, Y.; Johns, S. J.; Giacomini, K. M. Arginine 454 and lysine 370 are essential for the anion specificity of the organic anion transporter, rOAT3. *Biochemistry* **2001**, *40*, 5511−5520.

https://doi.org/10.1021/acsomega.2c04543
ACS Omega 2022, 7, 34621−34631